SEAKEEPING VALIDATION AND VERIFICATION USING DECOMPOSITION MODEL BASED ON EMBEDDED FREE SURFACE METHOD

Vuko Vukčević (Faculty of Mechanical Engineering and Naval Architecture, Croatia)
Hrvoje Jasak (Faculty of Mechanical Engineering and Naval Architecture, Croatia)

1 SUMMARY

Validation and verification of a KCS model in head seas is presented in this paper for five wave conditions. Validation is performed by comparing added resistance, heave and pitch motions with experimental data. Numerical model is verified via grid refinement studies, assessing grid uncertainty for each test case. Periodic uncertainty by means of moving window FFT is introduced and assessed. The decomposition model is based on SWENSE (Spectral Wave Explicit Navier–Stokes Equations) method and implicit relaxation zones. Jump conditions at the interface are used to obtain interface–corrected interpolation schemes for density and pressure, embedding the free surface into two single–phase equations for water and air. The method fully resolves issues with parasitic air velocities and ensures one–cell–sharp jump of dynamic pressure and density across the free surface. Implicitly redistanced Level Set equation is used for interface capturing, while the $k - \omega$ SST model is used for turbulence. The method is implemented in the `Naval Hydro pack` based on foam–extend, a fork of the open source software OpenFOAM.

2 INTRODUCTION

Due to recent regulations related to energy efficiency and green transport in the marine industry, Computational Fluid Dynamics (CFD) is gaining more attention. The focus in marine CFD slowly shifts from well validated steady resistance [7] to more complex problems such as seakeeping and manoeuvring [12]. One of the main challenges of great industrial importance is accurate assessment of added resistance of a ship in waves. Significant progress has been already achieved in this field [10], although verification studies are still scarce due to long simulation times. This paper presents validation and verification for seakeeping CFD simulations where each of the five test cases has been carried out, results compared to experimental data and verified by means of grid refinement studies, including grid and periodic uncer-

tainty assessment. Special attention is given to added resistance due to its practical importance.
The paper is organised as follows. Mathematical and numerical models are briefly outlined, followed by a brief description of uncertainty assessment. A global overview of the results is given and the paper is finalized with a short conclusion.

3 APPROACH

The computational method presented in this work is based on the recently developed decomposition model for naval hydrodynamics [13]. Decomposition is two–fold: solution decomposition is achieved with the SWENSE method [3], while the domain is decomposed with implicit relaxation zones [6] in order to prevent wave reflection. In SWENSE, only the perturbation around the approximate potential flow solution is solved, in contrast to solving for the full flow field.

Embedded free surface approach [14] allows us to formulate a single two–phase incompressible system of equations coupled at the interface via density and pressure jump conditions. Following Huang et al. [4], jump conditions are used to derive interface–corrected interpolation schemes for cells in the vicinity of the free surface. Reader is referred to Vukčević and Jasak [14] for a detailed derivation of jump conditions, two–phase governing equations and interface–corrected numerical schemes. Governing equations for the present decomposition model are:

- Volumetric continuity equation:

$$\nabla_{\bullet} \mathbf{u}_D = \mathcal{S}_{c.e.} , \qquad (1)$$

where $\mathbf{u}_D$ is the diffracted (perturbation) velocity field and $\mathcal{S}_{c.e.}$ represents explicit contribution arising from SWENSE decomposition [13], where index $c.e.$ stands for the continuity equation.

- Two–phase incompressible momentum equation:

$$\frac{\partial \mathbf{u}_D}{\partial t} + \nabla \bullet ((\mathbf{u} - \mathbf{u}_M)\mathbf{u}_D) - \nabla \bullet (\nu_{eff}\nabla \mathbf{u}_D)$$
$$= -\frac{1}{\rho}\nabla p_d + \mathcal{S}_{m.e.}, \quad (2)$$

where $\mathbf{u} = \mathbf{u}_D + \mathbf{u}_I$ is the total velocity field (diffracted + incident), while $\mathbf{u}_M$ is the relative grid motion velocity (flux) field arising from the Space Conservation Law [2] for moving grids. ν_{eff} is the effective kinematic viscosity allowing general turbulence modelling (RANS or LES) and ρ is the sharp density field yielding density of the water below the free surface and density of the air above the free surface. Both density and dynamic pressure p_d have jumps across the free surface which are taken into account by embedding approach [14]. $\mathcal{S}_{m.e.}$ is the explicit source term arising from SWENSE decomposition, including time derivative, convection and diffusion term for the incident velocity field.

- Implicitly redistanced Level Set (LS) equation:

$$\frac{\partial \psi_D}{\partial t} + \nabla \bullet ((\mathbf{c} - \mathbf{u}_M)\psi_D) - \nabla \bullet (b\nabla \psi_D)$$
$$= b\frac{\sqrt{2}}{\epsilon}\tanh\left(\frac{\psi}{\epsilon\sqrt{2}}\right) + \mathcal{S}_{l.s.e.}, \quad (3)$$

where ψ_D is the diffracted LS field and $\mathbf{c}$ is the convective flux field which works with diffusion and source terms to transport and maintain the signed distance function [13]. b is the diffusion coefficient and $\mathcal{S}_{l.s.e.}$ denotes explicit source term in the LS equation arising from the SWENSE decomposition, including time derivative, convection and diffusion term for the incident LS field. Hyperbolic tangent term in (3) is the explicit, non–decomposed source term.

Turbulence is modelled with two–equation $k - \omega$ SST model [8]. Along with governing equations for the two–phase flow field, following jump conditions are used at the free surface [4, 14].

- Dynamic pressure jump condition:

$$p_d^- - p_d^+ = -(\rho^- - \rho^+)\mathbf{g}\bullet\mathbf{x}, \quad (4)$$

where superscripts $+$ and $-$ denote field values infinitesimally close to the free surface from water and air sides, respectively. Similarly, ρ^- is the constant air density and ρ^+ is the constant water density. $\mathbf{g}$ is the gravitational acceleration and $\mathbf{x}$ is the free surface position vector.

- Dynamic pressure gradient jump condition:

$$\frac{1}{\rho^-}p_d^- - \frac{1}{\rho^+}p_d^+ = 0. \quad (5)$$

Jump condition given by Eqn. (4) is exact, while Eqn. (5) is obtained by approximating tangential stress balance and neglecting surface tension effects at the free surface. Such approximations are valid for large length–scale flows encountered in naval hydrodynamics [4].

Jump conditions (4) and (5) are used to derive interface–corrected interpolation schemes for dynamic pressure and density in the framework of second–order accurate polyhedral Finite Volume (FV) method [5]. As the polyhedral FV method uses a compact computational stencil, interface–corrected schemes are used only for cells in the immediate vicinity of the free surface, while ordinary discretisation is employed for fully submerged or fully dry cells. Time derivative terms for diffracted fields are discretised with first–order accurate implicit Euler scheme (due to stability issues on some grids), while time derivative terms for incident fields are discretised with a blend of Crank–Nicholson and Euler schemes. This combination proved to be accurate in previous studies. Convective terms for incident and diffracted fields are discretised with linear and linear upwind interpolation, respectively. All diffusion terms are discretised using linear interpolation with non–orthogonal correction in over–relaxed form [5]. Theoretically, second–order spatial accuracy and a blend of first– and second–order temporal accuracy is achieved.

Apart from the fluid flow equations, six–degrees–of–freedom (6 DOF) rigid body motion equations [1] are introduced, where the rotation is formulated in quaternion form to prevent the gimbal lock phenomenon. After the solution of 6 DOF equations, computational grid is moved as a rigid body and grid motion fluxes are calculated, where wave boundary conditions with relaxation zones naturally account for moving grids.

6 DOF and grid motion are tightly coupled to the fluid flow solution via forces and moments acting on the body, prescribed velocity of the body and grid motion fluxes. In order to resolve this coupling, fluid flow and 6 DOF equations are solved using Picard iterations. First, interface capturing equation (3) is solved, followed by a momentum equation (2). The pressure–velocity coupling for the current interface location is resolved in the inner PISO loop with 3 or 4 correctors.

After obtaining a converged flow field including turbulence, 6 DOF equations are solved and the grid is moved accordingly. With updated grid motion fluxes and velocity boundary conditions for the body, a new estimate of the flow field is calculated. The procedure is repeated at least 5 times to damp out oscillatory convergence of rigid body accelerations.

4 VALIDATION

Validation of the model is performed by simulating five head wave cases (C1 to C5, C1 being the shortest, smallest wave, C5 being the longest, highest wave) requested at the Workshop [9] for the KCS model at design Froude number, and comparing the added resistance, heave and pitch with experimental data. Reader is referred to Workshop's website [9] for detailed case settings and post processing instructions. Three unstructured grids are used with approximately: 600 000, 950 000 and 1 600 000 cells. Each grid has a symmetry plane, and extends approximately $1L_{PP}$ in front of the ship, $2.5L_{PP}$ behind the ship and $1.5L_{PP}$ from the portside. Results presented here are obtained by performing moving window FFT on temporal signals for the finest grid, while the verification study with grid and periodic uncertainty estimates is presented afterwards.

4.1 Added resistance

Mean value, first and second order harmonics of the total resistance coefficient are presented in Fig. 1 for all wave conditions given by wave length to length between perpendiculars (λ/L_{PP}) ratio. Only the mean value of resistance coefficient for the C3 case ($\lambda/L_{PP} \approx 1.15$) is available from experimental data due to resonance in the setup. Fig. 1 shows good overall agreement of simulation results (CFD) with experimental data (EXP). Mean value of resistance is over–predicted, while the first order is under–predicted for each case. Relative errors for the mean component drop from $\approx 16\%$ for the lowest λ/L_{PP} case (smallest wave height) to $\approx 5\%$ for the highest λ/L_{PP} case (largest wave height). The trend is similar for first order harmonics with relative error of $\approx 12\%$ for the highest λ/L_{PP} case. The trend of decreasing errors with longer and higher waves is expected as the grid resolution is not sufficient for lower λ/L_{PP} cases, which have small wave heights. For example, case C1 with $\lambda/L_{PP} \approx 0.65$ and wave height of $H_s = 0.062$ m has only 10 cells per wave height on the finest grid, while case C5 has approximately 23 cells. Time–evolution of the resistance coefficient is presented in Fig. 2 for the C5 case, which has the finest

relative grid resolution: largest number of cells per wave height and length. It can be seen that the simulation results are in good agreement with experimental data, indicating good agreement for the first order phase.

4.2 Heave motion

Mean value, first and second order harmonics of the dimensionless heave are presented in Fig. 3 for all wave conditions. The mean value of heave is slightly over–predicted for all wave conditions. Relative errors for first order heave are within 6% for all wave conditions except for the C1 case with smallest wave height where the relative error is 25%. Although very small, second order effects are also well–predicted. Time–evolution of dimensionless heave is presented in Fig. 4 for the C5 case, demonstrating good overall agreement with experimental data and indicating minor phase shift difference.

4.3 Pitch motion

Mean value, first and second order harmonics of the dimensionless pitch are presented in Fig. 5 for all wave conditions. As for the total resistance coefficient and heave motion, simulation results for the pitch motion correctly model the trend with increasing wave length, compared to experimental data. Relative errors for first order harmonic amplitudes are within 8% for the three longest and highest waves. C2 case with $\lambda/L_{PP} \approx 0.85$ has the largest error of 45% for the first order harmonic. Second order effects are well–predicted. Time–evolution of dimensionless pitch is presented in Fig. 6 for the C5 case, showing good agreement with experimental data and indicating minor phase shift difference as was the case for resistance and heave.

5 VERIFICATION

As the iterative uncertainty is low, we first examine periodic uncertainty and then calculate grid uncertainty, for each test case.

5.1 Periodic uncertainty assessment

Seakeeping CFD simulations are exclusively carried out in the time domain, where appropriate number of periods needs to be calculated. In highly non–linear flow problems such as seakeeping of a ship, minimum number of required periods needs to be assessed. For this reason, we perform a moving window FFT on
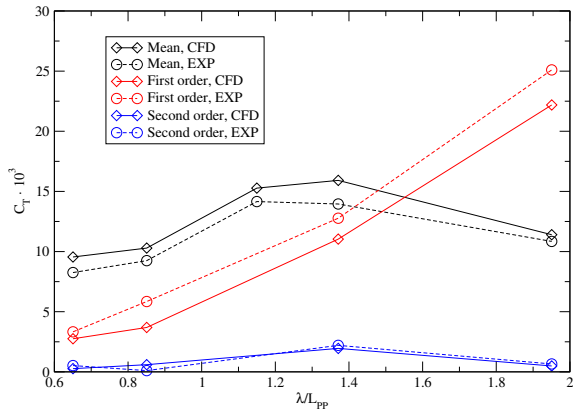
Figure 1: Total resistance coefficient harmonics, C_T for all wave conditions.
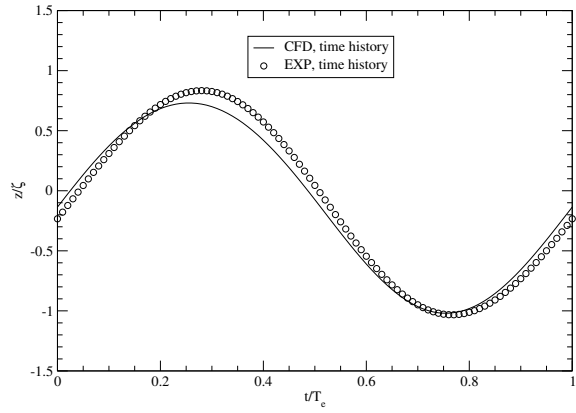

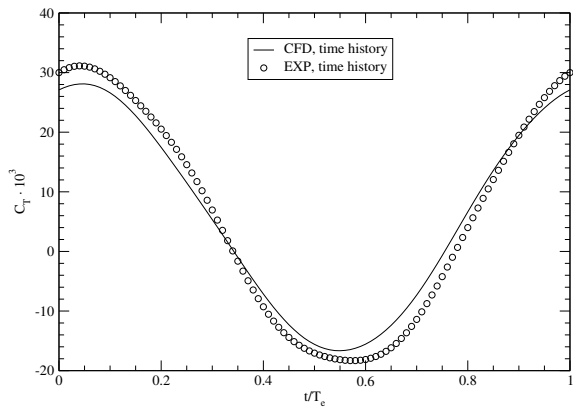Figure 4: Time history of dimensionless heave, z/ζ for the C5 case.

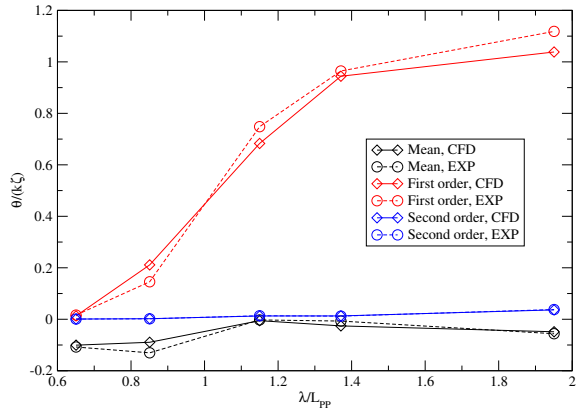Figure 2: Time history of the total resistance coefficient, C_T for the C5 case.

Figure 5: Dimensionless pitch harmonics, $\theta/(k\zeta)$ for all wave conditions.
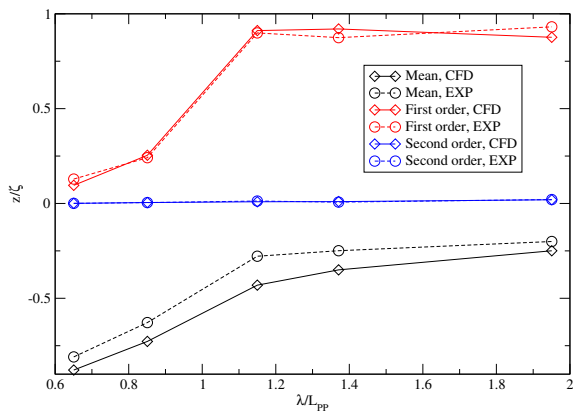

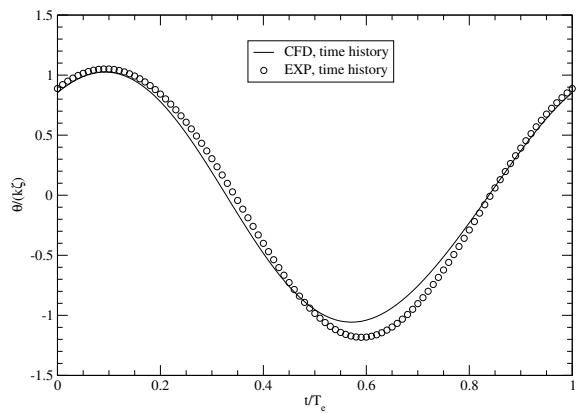Figure 3: Dimensionless heave harmonics, z/ζ for all wave conditions.

Figure 6: Time history of dimensionless pitch, $\theta/(k\zeta)$ for the C5 case.

each signal, which provides useful information about convergence of particular harmonics. Convergence of the mean total resistance coefficient for the C5 case is presented in Fig. 7. The convergence for all items (harmonic amplitudes and phases for resistance, heave and pitch, for all cases) is found to be oscillatory. Hence, we calculate periodic uncertainty in the same way as the oscillatory grid uncertainty [11]:

$$U_P = 0.5 |S_U - S_L|, \qquad (6)$$

where S_U is the maximum value, and S_L is the minimum value of the moving window FFT plot over the final region used for post processing, usually last 5 to 10 encounter periods.

Periodic uncertainties for the mean and first order harmonics of resistance, heave and pitch are less than 2% of the finest grid result. Higher order (third and fourth) harmonics for heave and pitch, have periodic uncertainties up to 50%. This is expected as higher order harmonic amplitudes of heave and pitch are approximately 3 orders of magnitude smaller than corresponding first orders. Periodic uncertainties for higher order harmonics could be lowered by simulating more encounter periods.

5.2 Grid uncertainty assessment

Grid convergence and uncertainty is assessed following guidelines by Stern et al. [11], using results from 3 (non–systematically) refined grids. A mixture of monotonically–, oscillatory– and non–converging solutions is obtained as in previous studies concerning seakeeping of the KCS ship [10]. Grid uncertainty could not be calculated for non–converging items.
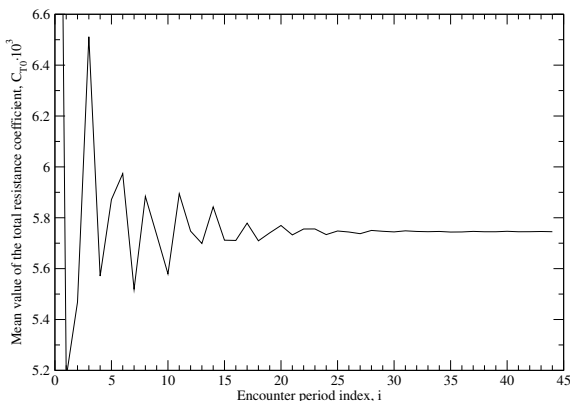

Figure 7: Moving window FFT plot for the mean total resistance coefficient, case C5.

5.2.1 Added resistance grid uncertainties

The average grid uncertainty U_G for the mean value of resistance is approximately 3.3% of the finest grid result. Grid uncertainty for the first order harmonic of the resistance is less than 2%, except for the resonant C3 case where $U_G = 12.5\%$. Higher order harmonics for the resistance have average uncertainty of 10%, with one outlier: third order harmonic amplitude of the C1 case, with $U_G = 65\%$.

5.2.2 Heave grid uncertainties

For the mean value of heave, grid uncertainty ranges from 0.4% for C1 case to 49% for resonant C3 case. Grid uncertainties for first order harmonics of heave are smaller than 2%, while higher order amplitudes have an average grid uncertainty of approximately 10.5%.

5.2.3 Pitch grid uncertainties

Pitch generally follows the same trend as heave: low grid uncertainties of approximately up to 2% for the mean value and 62% for resonant C3 case. Grid uncertainties for first order amplitudes of pitch are less than 2% for largest λ/L_{PP} cases, where for the two lowest cases, grid uncertainty could not be calculated due to non–converging solution. Higher order pitch amplitudes have an average grid uncertainty of approximately 11%.

5.2.4 General notes on grid convergence

Out of 75 harmonic amplitudes (mean to fourth order for resistance, heave and pitch, for each of the five cases), 64 exhibit monotone or oscillatory convergence with grid refinement, while 11 do not converge. Out of 11 non–converging items, 7 are clustered at low λ/L_{PP} cases where the grid resolution on all grids is insufficient for such small wave lengths and heights. 51 out of 60 phases exhibit convergence with grid refinement, with 5 of non–converging phases clustered at low λ/L_{PP} cases.

6 CONCLUSION

This paper describes a detailed validation and verification of the decomposition model with embedded free surface approach in added resistance simulations. The computational model is implemented in the `Naval Hydro pack` based on foam–extend C++ library, a community driven fork of OpenFOAM software.

Five test cases of the KCS ship model heaving and

pitching in head seas are simulated. Validation is performed by comparing mean to fourth order harmonics of added resistance, heave and pitch motions with experimental data, while the verification is performed via grid refinement studies and periodic uncertainty assessment.

Mean value of the added resistance in waves is well predicted, with relative error of 5% for the C5 case, which has the best relative grid resolution: highest number of cells per wave length and height. Grid uncertainties for the mean component of the added resistance are 3.3% on average, while periodic uncertainties are less than 2%. Relative errors for the first order harmonics of added resistance are slightly larger compared to mean value, with similarly low grid and periodic uncertainties.

Heave and pitch motions are also in good agreement with experimental data, with relative errors for first order harmonics usually below 8%. Exceptions with larger relative errors are clustered at low λ/L_{PP} cases with small wave heights and short wave lengths, which are more demanding from grid resolution point of view.

7 HARDWARE AND SIMULATION TIMES

Simulations were performed on a cluster with 6 nodes: CPU - 2x Intel Xeon E5-2637 v3 4-core, 3.5 GHz, 15MB L3 Cache, DDR4-2133. As an example, the finest grid (1.6 million cells) simulation of the resonant (C3) case has been performed using 40 cores. 7 motion correctors were used with fixed time step of 0.004 s corresponding to approximately 328 time steps per encounter period. Maximum CFL number was ranging from 25 to 45 during the simulation. Simulation lasted 23.5 hours (1 day) for 27.5 encounter periods, leading to 50 minutes of CPU time per encounter period.

References

[1] P. M. Carrica, R. V. Wilson, R. W. Noack, and F. Stern. Ship motions using single–phase level set with dynamic overset grids. *Comput. Fluids*, 36:1415–1433, 2007.

[2] I. Demiridžić and M Perić. Space conservation law in finite volume calculations of fluid flow. *Int. J. Numer. Meth. Fluids*, 8:1037–1050, 1998.

[3] P. Ferrant, L. Gentaz, and D. Le Touzé. A new RANSE/Potential Approach for Water Wave Diffraction. In *Proc. Numerical Towing Tank Symposium, NuTTS*, September 2002.

[4] J. Huang, P. M. Carrica, and F. Stern. Coupled ghost fluid/two–phase level set method for curvilinear body–fitted grids. *Int. J. Numer. Meth. Fluids*, 44:867–897, 2007.

[5] H. Jasak. *Error Analysis and Estimation for the Finite Volume Method with Applications to Fluid Flows*. PhD thesis, Imperial College of Science, Technology & Medicine, London, 1996.

[6] H. Jasak, V. Vukčević, and I. Gatin. Numerical Simulation of Wave Loads on Static Offshore Structures. In *CFD for Wind and Tidal Offshore Turbines*, pages 95–105. Springer Tracts in Mechanical Engineering, 2015.

[7] L. Larsson, F. Stern, and M. Vissoneau. *Numerical Ship Hydrodynamics: An assessment of the Gothenburg 2010 workshop*. Springer, 2013.

[8] F. R. Menter. Two-equation eddy-viscosity turbulence models for engineering applications. *AIAA J.*, 32(8):1598–1605, 1994.

[9] National Maritime Reasearch Inistitute (NMRI). Tokyo 2015: A Workshop on CFD in Ship Hydrodynamics. `http://www.t2015.nmri.go.jp/`, 2015. [Online; accessed 20 August 2015].

[10] C. D. Simonsen, J. F. Otzen, S. Joncquey, and F. Stern. EFD and CFD for KCS heaving and pitching in regular head waves. *J. Mar. Sci. Technol.*, 18:435–459, 2013.

[11] F. Stern, R. V. Wilson, H. W. Coleman, and E. G. Paterson. Comprehensive Approach to Verification and Validation of CFD Simulations– Part 1: Methodology and Procedures. *J. Fluids. Eng*, 123(4):793–802, 2001.

[12] F. Stern, J. Yang, Z. Wang, H. Sadat-Hosseini, M. Mousaviraad, Bhushan S., and T. Xing. Computational Ship Hydrodynamics: Nowadays and Way Forward. In *Proceedings of the 29th Symposium on Naval Hydrodynamics*, pages 1–73, August 2012.

[13] V. Vukčević and H. Jasak. Decomposition Model for Naval Hydrodynamic Applications, Part I: Computational Method. *Submitted to Ocean Engineering*, ??:???–???, 2015.

[14] V. Vukčević and H. Jasak. Embedded Free Surface Method in Polyhedral Finite Volume Framework: Part I: Computational Method. *Submitted to Journal of Computational Physics*, ??:???–???, 2015.